DRAFT VERSION JULY 19, 2016
Preprint typeset using LaTeX style emulateapj v. 5/2/11

arXiv:1605.00643v2 [astro-ph.GA] 16 Jul 2016

GALACTIC WINDS DRIVEN BY ISOTROPIC AND ANISOTROPIC COSMIC RAY DIFFUSION IN DISK GALAXIES

R. PAKMOR[1], C. PFROMMER[1], C. M. SIMPSON[1] AND V. SPRINGEL[1,2]

Draft version July 19, 2016

ABSTRACT

The physics of cosmic rays (CR) is a promising candidate for explaining the driving of galactic winds and outflows. Recent galaxy formation simulations have demonstrated the need for active CR transport either in the form of diffusion or streaming to successfully launch winds in galaxies. However, due to computational limitations, most previous simulations have modeled CR transport isotropically. Here, we discuss high resolution simulations of isolated disk galaxies in a $10^{11}\mathrm{M}_{\odot}$ halo with the moving mesh code AREPO that include injection of CRs from supernovae, advective transport, CR cooling, and CR transport through isotropic or anisotropic diffusion. We show that either mode of diffusion leads to the formation of strong bipolar outflows. However, they develop significantly later in the simulation with anisotropic diffusion compared to the simulation with isotropic diffusion. Moreover, we find that isotropic diffusion allows most of the CRs to quickly diffuse out of the disk, while in the simulation with anisotropic diffusion, most CRs remain in the disk once the magnetic field becomes dominated by its azimuthal component, which occurs after $\sim 300\,\mathrm{Myrs}$. This has important consequences for the gas dynamics in the disk. In particular, we show that isotropic diffusion strongly suppresses the amplification of the magnetic field in the disk compared to anisotropic or no diffusion models. We therefore conclude that reliable simulations which include CR transport inevitably need to account for anisotropic diffusion.

Subject headings: cosmic rays – galaxies: evolution – galaxies: magnetic fields

1. INTRODUCTION

Understanding the formation and evolution of galaxies is one of the most fascinating problems in modern cosmology. The observed galaxy luminosity and HI-mass functions have much shallower faint-end slopes than predicted by ΛCDM models; this is locally known as the 'missing satellites problem' of the Milky Way, which should contain many more dwarf-sized subhalos than observed (see Kravtsov 2010, for a review). Recent cosmological simulations have identified feedback in the form of galactic winds as being primarily responsible for solving this problem as well as for obtaining realistic rotation curves of disk galaxies and for enriching the intergalactic medium with metals (Schaye et al. 2010; Guedes et al. 2011; Puchwein & Springel 2013; Marinacci et al. 2013; Hopkins et al. 2014; Vogelsberger et al. 2014; Schaye et al. 2015). However, galactic winds in these simulations are often included as a phenomenological model. Their basic properties, such as the wind velocity or mass loading, are tuned to match observed global relations of galaxies. Ideally, we would like to directly simulate the physics responsible for the wind driving, but the exact nature of this physical origin is still strongly debated.

One popular idea is that momentum-driven winds could result from radiation pressure acting on dust grains and atomic lines in dense gas, imparting enough momentum to accelerate the gas, potentially explaining strong outflows in starburst galaxies (Murray et al. 2005; Thompson et al. 2005). However, direct radiation-hydrodynamics simulations of the Rayleigh-Taylor instability (Krumholz & Thompson 2012) and large-scale galaxy models (Rosdahl et al. 2015; Skinner & Ostriker 2015) fail to see strong, mass-loaded winds because the radiation is not sufficiently trapped (as assumed in more simplified analytical calculations) but instead generates a channel structure along which a substantial fraction of the radiation is able to escape.

CRs in galaxies have also been proposed to drive outflows in a number of theoretical works (Ipavich 1975; Breitschwerdt et al. 1991; Zirakashvili et al. 1996; Ptuskin et al. 1997; Breitschwerdt et al. 2002; Socrates et al. 2008; Everett et al. 2008, 2010; Samui et al. 2010; Dorfi & Breitschwerdt 2012) or by using three-dimensional simulations of the ISM (Hanasz et al. 2013; Girichidis et al. 2016). Polarized radio observations of edge-on galaxies show poloidal field lines at the disk-halo interface (e.g., Tüllmann et al. 2000). This argues for a dynamical mechanism that is responsible for reorienting the toroidal magnetic field in the disk and may be explained by a CR-driven Parker instability (Rodrigues et al. 2016). Indeed, recent hydrodynamical simulations of the formation and evolution of disk galaxies have shown that CR pressure can drive strong bipolar outflows in disk galaxies provided they are allowed to stream (Uhlig et al. 2012; Ruszkowski et al. 2016) or diffuse (Booth et al. 2013; Salem & Bryan 2014; Salem et al. 2014) relative to the rest frame of the gas. However, they also showed that injecting CRs at supernova remnants and only accounting for their advective transport is not sufficient for launching winds (Jubelgas et al. 2008; Pfrommer et al. 2016).

Most of these simulations treated CR transport in the isotropic approximation, even though it is clear that CRs are dominantly transported along magnetic field lines (Desiati & Zweibel 2014). Here, we present high resolution simulations of the formation and evolution of a disk galaxy in an isolated $10^{11}\mathrm{M}_{\odot}$ dark matter halo with isotropic as well as anisotropic diffusion and analyze the differences. We describe our methods and setup in §2. We then discuss differences in the properties of the gas disk and the outflow in §3. We analyze the magnetic field amplification in the disk for the different runs in §4 and end with a brief summary in §5.

[1] Heidelberger Institut für Theoretische Studien, Schloss-Wolfsbrunnenweg 35, 69118 Heidelberg, Germany
[2] Zentrum für Astronomie der Universität Heidelberg, Astronomisches Recheninstitut, Mönchhofstr. 12-14, 69120 Heidelberg, Germany

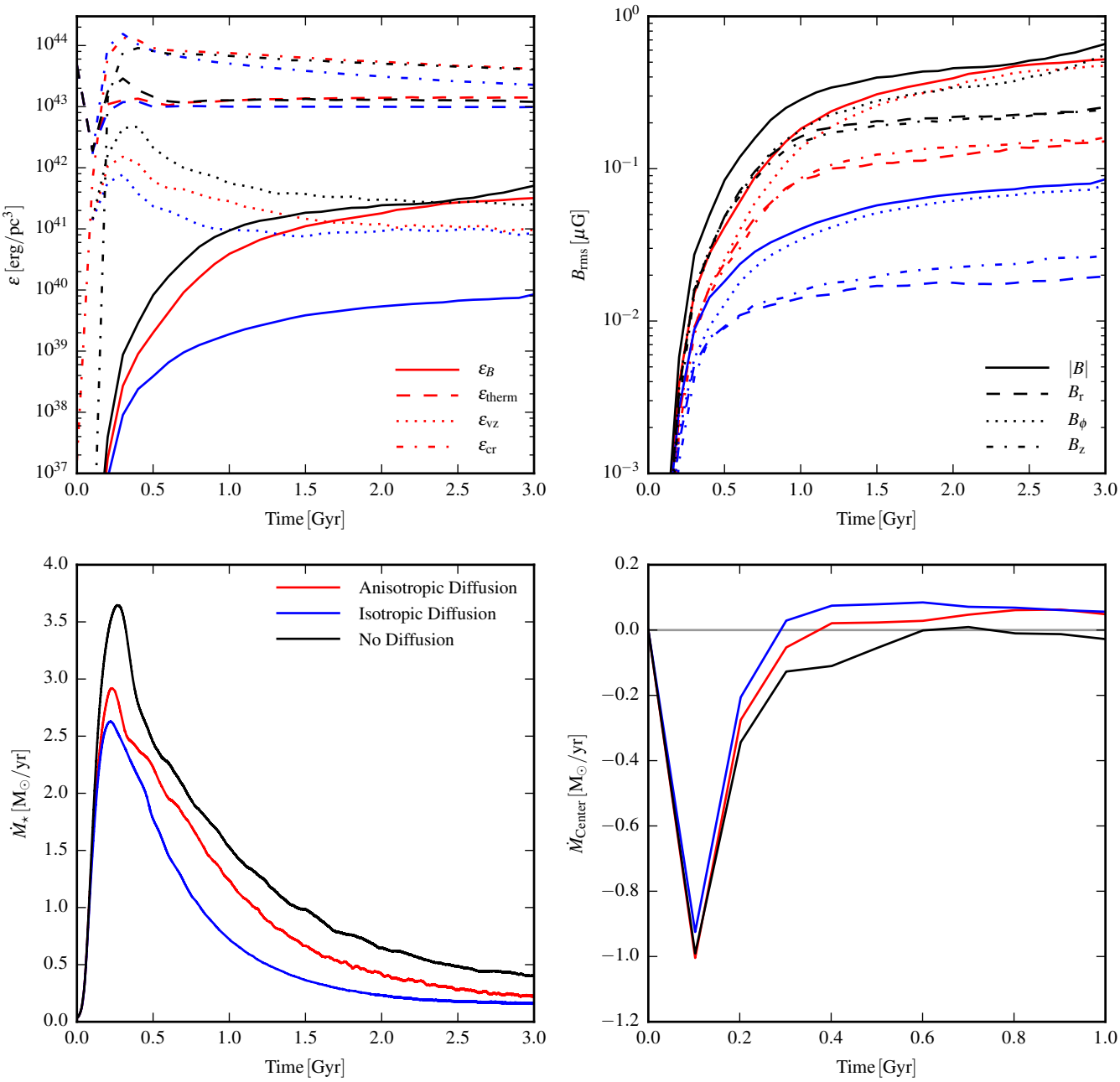

Figure 1. Evolution of different energy densities (top left), rms magnetic field strength (top right), star formation rate (bottom left), and the net vertical mass flux through a box of size 4 kpc centered on the galaxy (bottom right). Energies and magnetic field strength are measured in a cylindrical ring with inner radius 3 kpc, outer radius 10 kpc, and a height of 1 kpc centered on the midplane. The inner radius is chosen to cut out the strong central bipolar outflow. The top left shows the evolution of the average magnetic energy density, thermal energy density, kinetic energy density in vertical velocities, and CR energy density, respectively. The top right panel shows $B_{\rm rms}$ for the total magnetic field strength and the radial, azimuthal, and vertical components in cylindrical coordinates, respectively. The bottom right panel is only shown until $t = 1$ Gyr to emphasize the early evolution.

2. METHODS AND SETUP

We simulate the formation and evolution of an isolated disk galaxy in a 10^{11}M$_\odot$ halo with the moving-mesh code AREPO (Springel 2010). We use the new second order hydro scheme (Pakmor et al. 2016b). Cooling and star formation are modelled as described in Springel & Hernquist (2003). Magnetic fields are modelled with ideal MHD using cell-centered magnetic fields and the Powell scheme (Powell et al. 1999) for divergence control (Pakmor et al. 2011; Pakmor & Springel 2013).

CRs are modelled as a relativistic fluid with a constant adiabatic index of $4/3$ in the two fluid approximation (Pfrommer et al. 2016) [3]. To model the generation of CRs in supernova remnants from core-collapse supernovae, we inject 10^{48} erg

[3] Unlike Pfrommer et al. (2016) Sec. 3.3, here we use the collisional heating rate due to Coulomb interactions only, where $\Gamma_{\rm th} = -\Lambda_{\rm Coul} = \tilde{\lambda}_{\rm th} n_{\rm e} \varepsilon_{\rm cr}$ and $\tilde{\lambda}_{\rm th} = 2.78 \times 10^{-16}$ cm^3 s^{-1}.

of CR energy per solar mass of formed stars into the local environment of every newly created star particle. In contrast to similar work (Booth et al. 2013; Salem & Bryan 2014), we describe the thermal and kinetic energy injection with an effective equation of state (Springel & Hernquist 2003). We model CR cooling to thermal energy and radiation via Coulomb and hadronic interactions assuming an equilibrium distribution (Pfrommer et al. 2016). Moreover, in addition to advection of the cosmic ray fluid with the gas we include active CR transport relative to the gas rest frame in the form of isotropic or anisotropic diffusion (Pakmor et al. 2016a). For isotropic diffusion, we assume a constant isotropic diffusion coefficient of $10^{28}\mathrm{cm}^2\,\mathrm{s}^{-1}$. For anisotropic diffusion, we employ the same constant value parallel to the magnetic field and no diffusion perpendicular to it.

Our setup is very similar to the isolated disk setup described in Pakmor & Springel (2013). We model the dark matter halo as a static NFW (Navarro et al. 1996) density profile with a concentration parameter of 7.2. In this dark matter halo we put slowly rotating gas in hydrostatic equilibrium with a baryonic mass fraction of 0.17 and add rotation with a spin parameter of $\lambda = 0.05$. The magnetic field is initialized as a uniform homogeneous seed field along the x-axis with an initial field strength of $10^{-10}\,\mathrm{G}$. There are no CRs in the initial setup.

We start with about 10^7 gas cells with a target mass of $1.5 \times 10^3\,\mathrm{M}_\odot$, the same as the typical mass of a star particle. Using explicit refinement and de-refinement we enforce that the mass of all cells is within a factor of two of the target mass. Moreover, we require that adjacent cells differ by less than a factor of 10 in volume, otherwise the larger cell is also refined. We employ the standard mesh regularization scheme in AREPO (Vogelsberger et al. 2012; Pakmor et al. 2016b). In the following, we discuss 3 simulations with CRs that differ by either employing transport with isotropic diffusion, by using anisotropic diffusion, or by not including transport at all. Otherwise the simulations are identical.

3. DISK PROPERTIES

Initially in all of our simulations, the gas sphere immediately begins to cool, with the fastest cooling rates occurring at the dense center. The gas loses pressure support and collapses into a disk as it keeps its specific angular momentum. Once the gas density in the disk becomes high enough, stars are formed and CRs are injected for every star particle formed. Due to the resulting inhomogeneous cosmic ray distribution, the transport of CRs becomes important.

The star formation rate for all runs peaks around 300 Myr and then declines quickly, with most stars being formed in the first Gyr (see Figure 1). As the first stars form, the CR energy density in the disk quickly increases and is about 10 times as large as the thermal energy density when it peaks around 300 Myr. Later it declines again, mostly owing to cooling processes.

For our runs the star formation rate decreases with increasingly efficient diffusion. This effect is caused by CRs diffusing away from the center of the disk where most stars are formed. They reduce the flow of gas to the center as shown in Fig. 1. This is different to Salem & Bryan (2014) who found that diffusion increases the star formation rate. The discrepancy is likely a consequence of the different setup, as Salem & Bryan (2014) simulate the evolution of an existing disk which leads to much more distributed star formation.

Figure 2 shows the disk after 1.5 Gyr for the runs with isotropic and anisotropic diffusion. At this time, the gas densities in the disks are very similar in both runs. They strongly peak in the center of the disks, where most of the stars are formed and thus most of the CRs are injected. For the run with isotropic diffusion, they are then transported away in all directions and become quickly diluted into an almost spherical distribution. In contrast, with anisotropic diffusion, CRs can only be transported along magnetic field lines and therefore the diffusion process is very sensitive to the structure of the magnetic field.

The magnetic field strength is initially (in the first 300 Myr) amplified exponentially on very small timescales to a field strength of about $10^{-2}\,\mu$G (see top right panel in Figure 1), consistent with a turbulent small-scale dynamo. After this initial phase the disk has formed and the differential rotation in the disk dominates the velocity field. The magnetic field continues to grow exponentially, but on much longer timescales, indicating that the dominant amplification mechanism has changed. Around that time, the structure of the magnetic field also changes from a chaotic small-scale field to one completely dominated by its azimuthal component (see right panel in Figure 2). Note that even though the magnetic field is essentially completely aligned with the velocity field, it features a large number of field reversals, a behavior that is clearly different to our previous results for more massive halos (Pakmor & Springel 2013). We will explore this interesting dependence of the magnetic field structure on halo mass in a separate publication.

For the simulation with anisotropic diffusion, this magnetic field structure means that within the first 300 Myrs, the CRs diffuse essentially isotropically, but with a significantly lower effective diffusion coefficient as they are not transported along straight lines on large scales. Afterwards, however, they are mostly trapped at their radial and vertical positions and are only carried along the angular coordinate. Thus, a much larger fraction of the injected CRs remains in the disk as compared to the run with isotropic diffusion. Also, the run with anisotropic diffusion is more similar to the simulation without any diffusion in terms of the overall population of CRs in the disk.

Perhaps the strongest indication of a difference in the dynamic state of the gas in the disk for the different types of diffusion can be seen in the strength of the magnetic field. After 1.5 Gyrs, the typical magnetic field strength in the anisotropic diffusion run is about $1\,\mu$G. In contrast, in the isotropic diffusion run it only reaches a field strength of order $0.1\,\mu$G by this time. Since the structure of the magnetic field is very similar in both runs, it appears that either the same amplification mechanism works with different efficiencies in the two runs, or that different amplification mechanisms dominate in the two runs.

Even though the total energy in CRs in the disk is very similar for the runs with anisotropic diffusion and without diffusion, the effect of the CRs is rather different with respect to outflows. As shown in Figure 3, both simulations with diffusion develop strong centralized bipolar outflows, comparable to previous simulations of isolated disks with isotropic diffusion (Salem & Bryan 2014; Booth et al. 2013). The wind is driven by the vertical CR pressure gradient in the outer layers of the disk. At early times $t < 200$ Myr, its effect is very similar for both diffusion runs (see Fig. 1). Later, the magnetic field becomes dominated by its azimuthal component, and vertical CR diffusion is suppressed by a factor of ≈ 10 for the anisotropic diffusion run. Its outflow fully develops

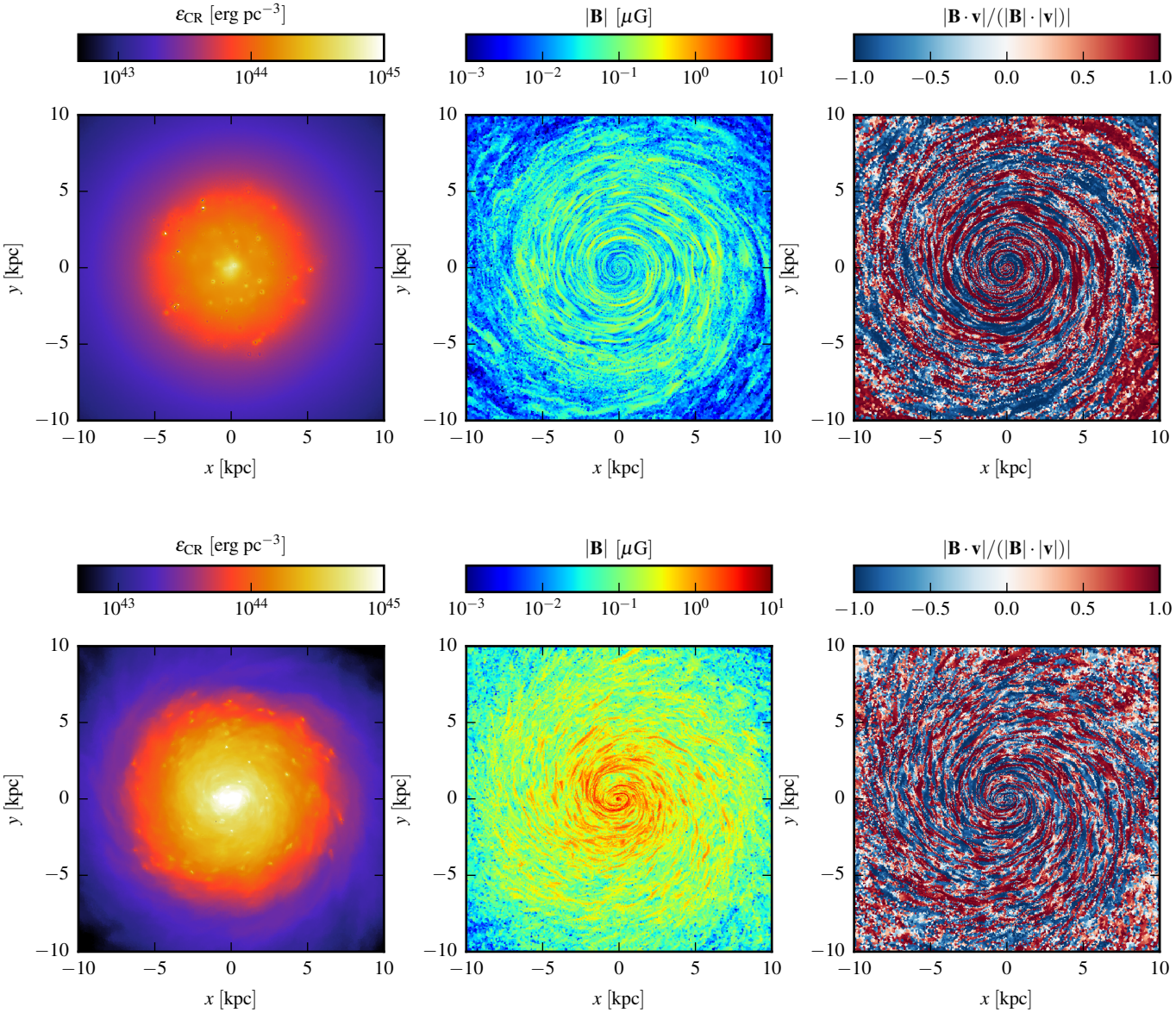

Figure 2. Properties of the gas disk after 1.5 Gyrs for the runs with isotropic CR diffusion (top row) and anisotropic CR diffusion (bottom row). The columns show slices in the midplane of the disk. From left to right, the color-coded maps show the CR energy density, the magnetic field strength, and the cosine of the angle between the directions of the magnetic field and the velocity field.

after 800 Myr; by contrast, only 400 Myr are needed in the isotropic diffusion run.

After 1.5 Gyr, the outflows have mass loading factors of 1.0 (measured at a height of 5 kpc above and below the disk and within a radius of 10 kpc) and 1.1 in the runs with anisotropic diffusion and isotropic diffusion, respectively, broadly consistent with previous results for Milky Way like massive halos (Salem & Bryan 2014; Booth et al. 2013).

The run without diffusion does not develop any large scale outflows. Instead, it shows a strong fountain flow up to a height of 2-3 kpc. This fountain flow is also present in the diffusion runs, but is suppressed in the simulation with isotropic diffusion. In this calculation, the vertical velocity field in the disk (excluding the bipolar outflow) seems to be generally lower and lacks small-scale structure. Note that in both diffusion runs we additionally see what looks like a large-scale fountain flow over the disk, outside the central outflow, that reaches beyond 10 kpc in height.

4. MAGNETIC FIELD AMPLIFICATION

As discussed above, the amplification timescales of the magnetic field strength deviate after an initial period of small-scale turbulent amplification in the two runs with isotropic and anisotropic diffusion. At the same time, the azimuthal component of the magnetic field starts to dominate over the vertical and radial components in all runs, even though initially all three components of the magnetic field were of equal strength. This indicates a change in the dominant amplification mechanism from small-scale turbulent amplification to a large-scale dynamo.

An analytical model to describe magnetic field amplification in an axisymmetric disk has been proposed by Shukurov et al. (2006). In this model, the mean radial field $\bar{B}_r$ and mean

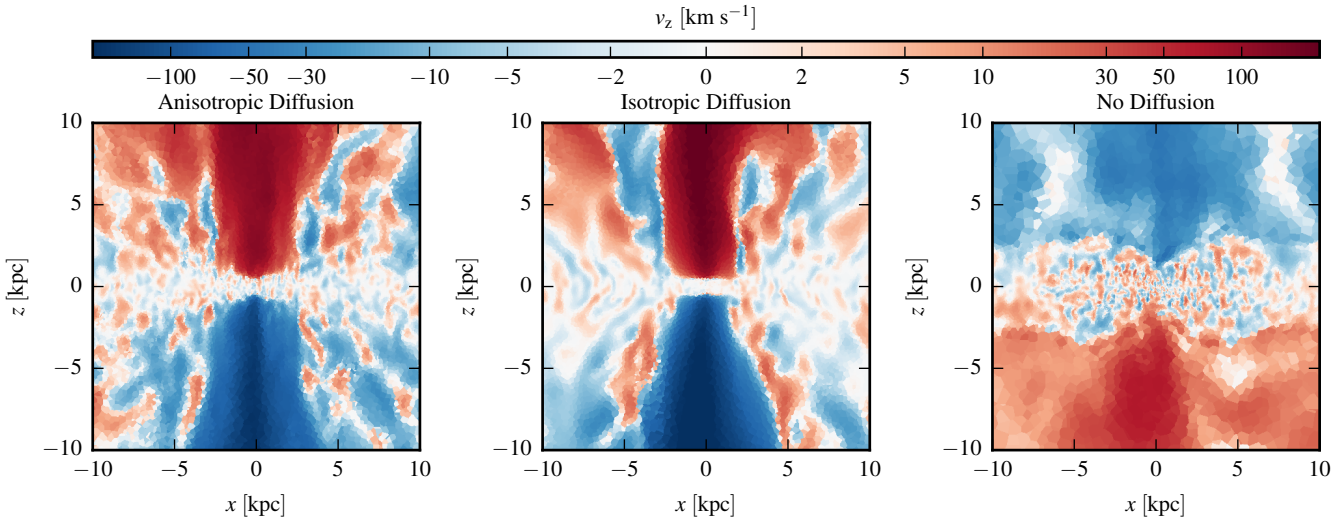

Figure 3. Slices in the $x-z$ plane through the center of the disk of the, showing the z-velocity component after 1.5 Gyr. The columns from left to right correspond to the simulations with anisotropic CR diffusion, isotropic CR diffusion, and without CR diffusion, respectively.

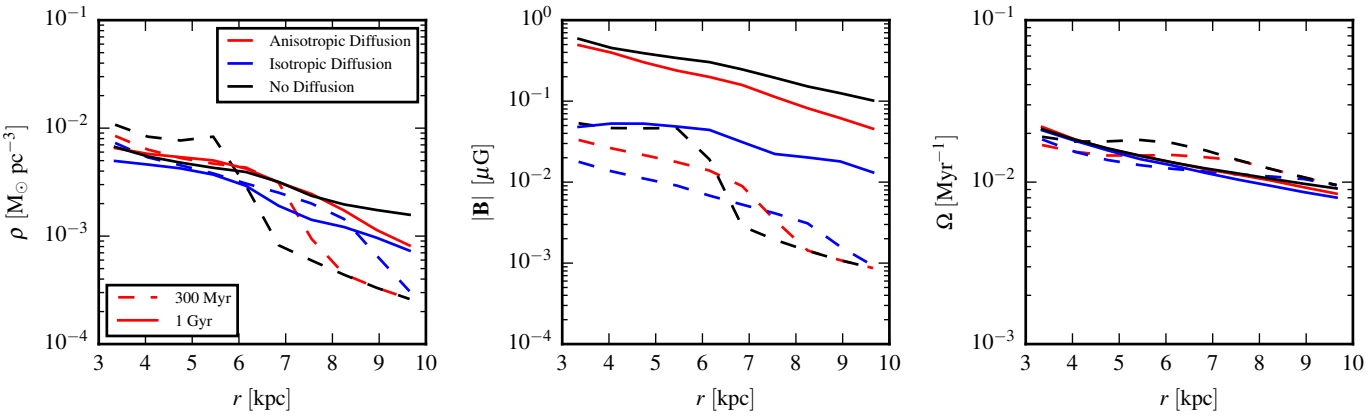

Figure 4. Radial profiles of volume weighted mean gas density, root mean square magnetic field strength, and angular velocity in a cylinder with a height of 8 kpc centered on the midplane of the disk for the runs with anisotropic diffusion (black), isotropic diffusion (red), and without diffusion (blue), for two different times corresponding to 300 Myrs (dashed lines) and 1.0 Gyrs (solid lines), respectively.

azimuthal field $\bar{B}_\phi$ in cylindrical coordinates change as

$$\frac{\partial \bar{B}_r}{\partial t} = -\frac{\partial}{\partial z}\left(\bar{v}_z \bar{B}_r + \mathcal{E}_\phi\right), \tag{1}$$

$$\frac{\partial \bar{B}_\phi}{\partial t} = -\frac{\partial}{\partial z}\left(\bar{v}_z \bar{B}_\phi + \mathcal{E}_r\right) + q\Omega_0 \bar{B}_r, \tag{2}$$

where $\bar{v}_z$ is the mean vertical velocity in the disk, $\mathcal{E}_r$ and $\mathcal{E}_\phi$ are the radial and azimuthal components of the turbulent electric field, and Ω_0 and q parameterize the angular velocity as $\Omega(r) = \Omega_0 r^q$. Here, we already neglected additional terms containing ohmic diffusion, as assumed by ideal MHD in our simulations.

The angular velocity shown in Figure 4 can be well described by a power law that it is very similar for all runs. Therefore, it cannot explain the differences in the observed amplification timescales of the magnetic field. Note that the magnetic field strength already differs by a factor of two at 300 Myrs between the runs with isotropic and anisotropic diffusion.

To estimate the importance of the remaining terms in the galactic dynamo equations above, we show the vertical profiles of the total magnetic field strength, mean vertical velocity, and $\bar{v}_z\bar{B}_r$ and $\bar{v}_z\bar{B}_\phi$ in Figure 5. At 300 Myrs, when the magnetic field strength starts to diverge, the vertical velocities close to the disk are still very similar in all three runs. However, the gradients in the strength of the radial and vertical magnetic field are shallower for the isotropic diffusion run as some highly magnetized gas has been pushed vertically out of the disk. Therefore, the amplification terms are smallest for the run with isotropic diffusion. The largest amplification terms are present for the run without diffusion. It also has the strongest gradients in the magnetic field strength as there is no significantly magnetized material above a height of 2 kpc.

The situation is very similar after 1.5 Gyrs. Now the magnetic field strength has mostly saturated for the runs without diffusion and with anisotropic diffusion, as the magnetic energy has become comparable to the kinetic energy in the vertical component of the velocity field. The still ongoing amplification is sufficient to compensate losses by numerical diffusion of the magnetic field and by the transport of magnetized gas out of the disk. In the run with isotropic diffusion the magnetic field strength is one order of magnitude smaller. It still increases slowly, but steadily, until its energy approaches

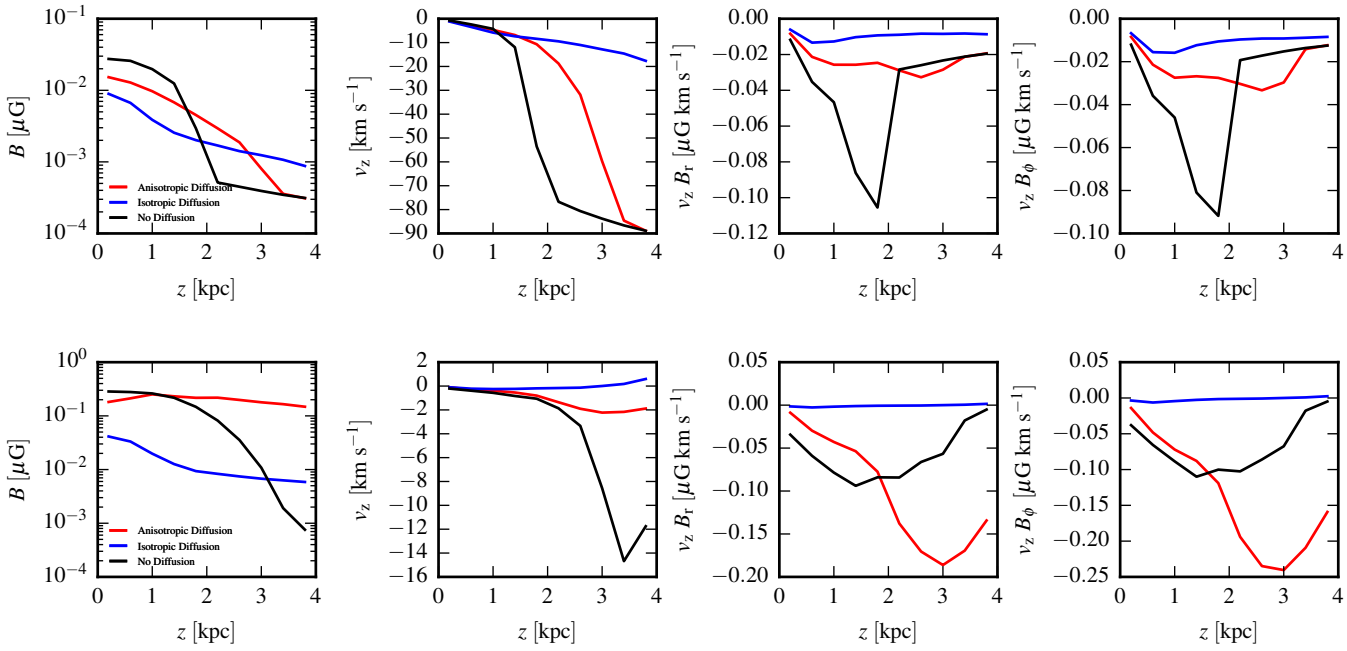

Figure 5. Vertical profiles of volume weighted mean gas properties in a cylindrical ring with an inner radius of 3 kpc and an outer radius of 10 kpc, after 300 Myrs (top row) and 1.0 Gyrs (bottom row), for the runs with anisotropic diffusion (black), isotropic diffusion (red), and without diffusion (blue). From left to right, the columns show total magnetic field strength, vertical velocity, vertical velocity times radial magnetic field strength, and vertical velocity times azimuthal magnetic field strength, respectively.

the vertical kinetic energy after about 10 Gyrs.

Note that even though the galactic dynamo model seems to do a good job in explaining the amplification of the magnetic field strength in our simulations as well as the qualitative differences between the runs, it is important to point out that its applicability is not obvious, as the large-scale magnetic field has many local field reversals that make the definition and interpretation of a mean magnetic field difficult. We also note that we do not model ohmic diffusion, therefore all magnetic diffusion is due to numerical dissipation effects on the grid scale.

5. SUMMARY

In this work, we focussed on the impact of different CR transport processes in simulations of isolated disk galaxies. For clarity, we studied the same initial conditions with isotropic diffusion and with anisotropic diffusion based on our newly developed solver. In addition, we also applied to this set-up a model that does not explicitly account for diffusion processes.

Our simulation outcomes with isotropic diffusion are consistent with previous results. However, we find that with anisotropic diffusion, CRs are initially mostly confined to the disk due to the predominantly azimuthal magnetic field, such that they end up being distributed similarly to the run without any diffusion. Moreover, we find that there are significant secondary differences in the disk gas dynamics between the runs with isotropic diffusion and anisotropic diffusion. In particular, the isotropic diffusion run strongly suppresses the magnetic field amplification and needs almost a Hubble time until the magnetic field strength saturates. In comparison, in the simulations with anisotropic diffusion and without diffusion, the field already saturates after around 1 Gyr.

Given these differences, we conclude that it is important to model the full anisotropic nature of CR transport, because the isotropic approximation can produce qualitatively and quantitatively incorrect results. It also seems likely that a similar conclusion holds for the more general case of CR streaming. This process has been included in simulations of galaxy formation for the first time by Uhlig et al. (2012), but in an isotropic fashion. Very recently, Ruszkowski et al. (2016) presented the first attempt of an anisotropic treatment. As our results confirm, this is clearly a very interesting research direction for future work on galaxy formation and evolution.

This work has been supported by the European Research Council under ERC-StG grant EXAGAL-308037, ERC-CoG grant CRAGSMAN-646955, and by the Klaus Tschira Foundation. VS acknowledges support through subproject EXAMAG of the Priority Programme 1648 “Software for Exascale Computing” of the German Science Foundation.

REFERENCES

Booth, C. M., Agertz, O., Kravtsov, A. V., & Gnedin, N. Y. 2013, ApJ, 777, L16
Breitschwerdt, D., Dogiel, V. A., & Völk, H. J. 2002, A&A, 385, 216
Breitschwerdt, D., McKenzie, J. F., & Voelk, H. J. 1991, A&A, 245, 79
Desiati, P., & Zweibel, E. G. 2014, ApJ, 791, 51
Dorfi, E. A., & Breitschwerdt, D. 2012, A&A, 540, A77
Everett, J. E., Schiller, Q. G., & Zweibel, E. G. 2010, ApJ, 711, 13
Everett, J. E., Zweibel, E. G., Benjamin, R. A., et al. 2008, ApJ, 674, 258
Girichidis, P., Naab, T., Walch, S., et al. 2016, ApJ, 816, L19
Guedes, J., Callegari, S., Madau, P., & Mayer, L. 2011, ApJ, 742, 76
Hanasz, M., Lesch, H., Naab, T., et al. 2013, ApJ, 777, L38
Hopkins, P. F., Kereš, D., Oñorbe, J., et al. 2014, MNRAS, 445, 581
Ipavich, F. M. 1975, ApJ, 196, 107
Jubelgas, M., Springel, V., Ensslin, T., & Pfrommer, C. 2008, A&A, 481, 33
Kravtsov, A. 2010, Advances in Astronomy, 2010, 281913
Krumholz, M. R., & Thompson, T. A. 2012, ApJ, 760, 155
Marinacci, F., Pakmor, R., & Springel, V. 2013, MNRAS
Murray, N., Quataert, E., & Thompson, T. A. 2005, ApJ, 618, 569
Navarro, J. F., Frenk, C. S., & White, S. D. M. 1996, ApJ, 462, 563

Pakmor, R., Bauer, A., & Springel, V. 2011, MNRAS, 418, 1392
Pakmor, R., Pfrommer, C., Simpson, C. M., Kannan, R., & Springel, V. 2016a, ArXiv e-prints
Pakmor, R., & Springel, V. 2013, MNRAS, 432, 176
Pakmor, R., Springel, V., Bauer, A., et al. 2016b, MNRAS, 455, 1134
Pfrommer, C., Pakmor, R., Schaal, K., Simpson, C. M., & Springel, V. 2016, ArXiv e-prints
Powell, K. G., Roe, P. L., Linde, T. J., Gombosi, T. I., & De Zeeuw, D. L. 1999, Journal of Computational Physics, 154, 284
Ptuskin, V. S., Voelk, H. J., Zirakashvili, V. N., & Breitschwerdt, D. 1997, A&A, 321, 434
Puchwein, E., & Springel, V. 2013, MNRAS, 428, 2966
Rodrigues, L. F. S., Sarson, G. R., Shukurov, A., Bushby, P. J., & Fletcher, A. 2016, ApJ, 816, 2
Rosdahl, J., Schaye, J., Teyssier, R., & Agertz, O. 2015, MNRAS, 451, 34
Ruszkowski, M., Yang, H.-Y. K., & Zweibel, E. 2016, ArXiv e-prints, 1602.04856
Salem, M., & Bryan, G. L. 2014, MNRAS, 437, 3312
Salem, M., Bryan, G. L., & Hummels, C. 2014, ApJ, 797, L18
Samui, S., Subramanian, K., & Srianand, R. 2010, MNRAS, 402, 2778
Schaye, J., Dalla Vecchia, C., Booth, C. M., et al. 2010, MNRAS, 402, 1536
Schaye, J., Crain, R. A., Bower, R. G., et al. 2015, MNRAS, 446, 521
Shukurov, A., Sokoloff, D., Subramanian, K., & Brandenburg, A. 2006, A&A, 448, L33
Skinner, M. A., & Ostriker, E. C. 2015, ApJ, 809, 187
Socrates, A., Davis, S. W., & Ramirez-Ruiz, E. 2008, ApJ, 687, 202
Springel, V. 2010, MNRAS, 401, 791
Springel, V., & Hernquist, L. 2003, MNRAS, 339, 289
Thompson, T. A., Quataert, E., & Murray, N. 2005, ApJ, 630, 167
Tüllmann, R., Dettmar, R.-J., Soida, M., Urbanik, M., & Rossa, J. 2000, A&A, 364, L36
Uhlig, M., Pfrommer, C., Sharma, M., et al. 2012, MNRAS, 423, 2374
Vogelsberger, M., Sijacki, D., Kereš, D., Springel, V., & Hernquist, L. 2012, MNRAS, 425, 3024
Vogelsberger, M., Genel, S., Springel, V., et al. 2014, MNRAS, 444, 1518
Zirakashvili, V. N., Breitschwerdt, D., Ptuskin, V. S., & Voelk, H. J. 1996, A&A, 311, 113